

## Measuring myofiber orientations from high-frequency ultrasound images using multiscale decompositions

This content has been downloaded from IOPscience. Please scroll down to see the full text.

2014 Phys. Med. Biol. 59 3907

(<http://iopscience.iop.org/0031-9155/59/14/3907>)

View [the table of contents for this issue](#), or go to the [journal homepage](#) for more

Download details:

IP Address: 170.140.64.213

This content was downloaded on 01/07/2014 at 16:34

Please note that [terms and conditions apply](#).

# Measuring myofiber orientations from high-frequency ultrasound images using multiscale decompositions

Xulei Qin<sup>1</sup> and Baowei Fei<sup>1,2,3,4</sup>

<sup>1</sup> Department of Radiology and Imaging Sciences, Emory University, Atlanta, GA 30329, USA

<sup>2</sup> Department of Mathematics and Computer Science, Emory University, Atlanta, GA 30329, USA

<sup>3</sup> Winship Cancer Institute of Emory University, Atlanta, GA 30329, USA

<sup>4</sup> The Joint Department of Biomedical Engineering, Emory University and Georgia Institute of Technology, Atlanta, GA 30329, USA

E-mail: [bfei@emory.edu](mailto:bfei@emory.edu)

Received 13 February 2014, revised 20 May 2014

Accepted for publication 2 June 2014

Published 24 June 2014

## Abstract

High-frequency ultrasound (HFU) has the ability to image both skeletal and cardiac muscles. The quantitative assessment of these myofiber orientations has a number of applications in both research and clinical examinations; however, difficulties arise due to the severe speckle noise contained in the HFU images. Thus, for the purpose of automatically measuring myofiber orientations from two-dimensional HFU images, we propose a two-step multiscale image decomposition method. It combines a nonlinear anisotropic diffusion filter and a coherence enhancing diffusion filter to extract myofibers. This method has been verified by ultrasound data from simulated phantoms, excised fiber phantoms, specimens of porcine hearts, and human skeletal muscles *in vivo*. The quantitative evaluations of both phantoms indicated that the myofiber measurements of our proposed method were more accurate than other methods. The myofiber orientations extracted from different layers of the porcine hearts matched the prediction of an established cardiac mode and demonstrated the feasibility of extracting cardiac myofiber orientations from HFU images *ex vivo*. Moreover, HFU also demonstrated the ability to measure myofiber orientations *in vivo*.

Keywords: ultrasound imaging, myofiber orientation, multiscale decomposition

(Some figures may appear in colour only in the online journal)

## 1. Introduction

Muscles in the human body perform the important functions of supporting movement, maintaining posture and circulating blood throughout the body. The imaging and quantification of their structure can aid in the diagnosis of normal and pathological muscle tissues. In particular, the quantitative assessment of fiber orientations from medical images is an important issue in both research and clinical examinations (Fleming *et al* 2008, Cetingul *et al* 2008, Pillen and van Alfen 2011), because fiber orientations are crucial to determining the properties of motion in the human body such as heart beats, breathing, eating or simply walking (Shi *et al* 2008).

In recent years, there has been an increase in the utilization of ultrasound imaging to assess human muscles in both static and dynamic conditions (Sengupta *et al* 2006, Shi *et al* 2008, Miyoshi *et al* 2009, Krogh *et al* 2013). As a noninvasive imaging modality, ultrasound has been widely used in different examinations and assessments (Qin *et al* 2011, 2013a, Akbari and Fei 2012, Fei *et al* 2012). It has also utilized in the imaging of injury or abnormal skeletal muscles (Krogh *et al* 2013, Mademli and Arampatzis 2005, Kiesel *et al* 2007), modeling and rebuilt skeletal muscle structure (Fukunaga *et al* 1997, Hodges *et al* 2003), and movement detection through the measurement of muscle states (Miyoshi *et al* 2009). Besides these efforts in muscle imaging, additional work has been done to quantify myofiber orientations in ultrasound images. Traditionally, the myofiber quantifications were conducted by manually drawing lines in the images, which was time-consuming and subjective. Therefore, Zhou and Zheng proposed an automatic estimation method based on a revolving Hough transform to extract muscle fibers in musculoskeletal ultrasound images (Zhou and Zheng 2008). In addition to the orientation, the muscle fiber movements in an ultrasound image series could also be automatically detected to analyze human movements (Miyoshi *et al* 2009). Another approach, different from these direct measurements, was proposed to first enhance fiber structures by reducing the speckle noise in the ultrasound images (Dutt and Greenleaf 1996, Yu and Acton 2002, Yongjin and Yong-Ping 2009). The myofiber orientations were then extracted by edge detection from the speckle denoised images. Unfortunately, it is still difficult to quantify small myofiber orientations in clinical ultrasound images, especially for cardiac imaging. The relatively lower ultrasound frequency (<20 MHz) leads to lower imaging resolution and makes it difficult to quantify cardiac myofiber orientation.

On the other hand, high-frequency ultrasound (HFU) with a frequency of higher than 20 MHz, which can offer high-resolution and high-quality images (Filoux *et al* 2011), has been applied to imaging small-scale tissue structures in different clinical applications such as ophthalmology (Bedi *et al* 2006, Martius *et al* 2010), dermatology and intravascular ultrasound (Foster *et al* 2009, 2011, Moran *et al* 2011). There have also been efforts to image myofibers using HFU (Bellah 2001, Qin *et al* 2013b). It has been utilized as a convenient, practical, and inexpensive method for evaluating a variety of musculoskeletal disorders in pediatric patients (Bellah 2001). Qin *et al* validated the feasibility of using HFU to image the cardiac fibers of porcine hearts *in vitro* (Qin *et al* 2013b). However, current quantification methods have problems in measuring small myofiber orientations from these ultrasound images because HFU leads to a vast number of scatter points in the images (Crosby *et al* 2009). These speckles easily disrupt the myofiber structures in HFU images. Because of their small size, previous denoising filters, such as NADFs and speckle reducing anisotropic diffusion filters (SRNDFs) (Yu and Acton 2002), smoothed the images by considering these small myofibers as noise and then eliminating them, and by enhancing the contrast among different tissue regions in a larger scale. On the other hand, if the speckles are not processed, the direct edge detection methods will take the speckle edges for fiber boundaries, which extracts the wrong fiber orientations.

Therefore, we proposed an automatic myofiber extraction method based on multiscale image decompositions in order to accurately extract the myofiber orientations from the HFU images. The combination of multiscale decomposition and various filtering has been an active research area in image processing (Subr *et al* 2009, Choudhury and Medioni 2011, Nilufar *et al* 2012) and has been applied to medical image enhancement and analysis (Galun *et al* 2007, Paquin *et al* 2009, Wang and Fei 2009, Tang and Tang 2012). In contrast to other approaches, our proposed myofiber extraction method contains a two-step multiscale image decomposition: (1) nonlinear anisotropic diffusion filtering (NLADF) (Perona and Malik 1990, Gerig *et al* 1992), and (2) coherence enhancing diffusion filtering (CEDF) (Weickert 1999, Burgeth *et al* 2009). This method can decrease the speckle noise while enhancing the myofiber structures.

This paper is organized as follows: section 2 describes the automatic myofiber orientation measurement method; section 3 describes the validation results on fiber-structure phantoms and on myofiber ultrasound images; discussion and conclusions are summarized in section 4.

## 2. Methods

### 2.1. HFU scanners and data acquisition

An imaging system (Vevo 2100, VisualSonics, Toronto, Canada) was used in this study. The ultrasound scanner was a dedicated, high-resolution system for pre-clinical research applications. Its ultra-high-frequency transducers had superior resolution and image uniformity through the entire field of view. The system had been used in small animal imaging for cardiovascular, epidermal, and ophthalmologic applications. One of its linear ultrasound probe with a central frequency of 40 MHz (Model MS550D) was used to image the cardiac fiber orientations. Another linear probe with a central frequency of 21 MHz (Model MS250) was applied to image skeletal muscles in human subjects.

First, in order to test the cardiac myofiber imaging, fresh porcine hearts were utilized in three different steps. A left ventricle (LV) free wall was cut into triangle shapes with a size of 12 mm × 10 mm × 3 mm. After the specimen was imaged by the MS550D 40 MHz probe, it was fixed and processed histologically. Second, a specimen from the LV free wall was split along the cardiac muscle direction into small bunches around 0.6–1 mm in diameter. These small bunches were settled in distilled water and then imaged by the MS550D 40 MHz probe. Finally, specimens from the LV free wall, LV apex, septum wall, and right ventricle (RV) free wall were excised and imaged by the 40 MHz probe. During imaging, the probe was attached to the cut surface of the specimens and was rotated to image the fiber structures. The imaging parameters of these three steps were set as 40 MHz frequency, 14.08 mm × 10 mm imaging region, and 256 line density.

For the purpose of skeletal myofiber imaging, the MS250 21 MHz ultrasound probe was first placed on the right calf of a human subject and adjusted to image the clear gastrocnemius fibers. Then it was utilized to image the brachioradialis muscles in the left arm. The imaging parameters were set as 21 MHz frequency, 18 mm × 24 mm imaging region, and 256 line density.

### 2.2. Myofiber simulation

In order to quantitatively analyze the proposed method, different simulated HFU images are generated by Field II (Jensen and Svendsen 1992), which linearly calculated the impulse response at all scatterer positions. Two different myofiber phantoms and corresponding

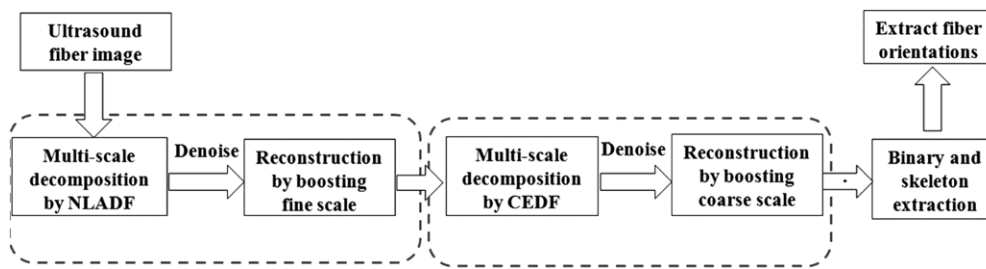


Figure 1. Flowchart of the proposed myofiber extraction method.

imaging parameters are set to simulate the HFU images of 21 MHz and 40 MHz linear probes, respectively.

For the 21 MHz probe, its phantom is set as follows: the whole volume is  $20 \text{ mm} \times 25 \text{ mm} \times 10 \text{ mm}$  and 30 scatterers per  $\text{mm}^3$  are randomly distributed in it. Five skeletal myofibers are set with the size of 4 mm in length and 0.1 mm in diameter. Three different reflection amplitudes of myofiber scatterers that are three, five, and ten times higher than those of background are chosen to set different quality images. Similarly, for the 40 MHz simulation, its phantom volume is  $16 \text{ mm} \times 12 \text{ mm} \times 6 \text{ mm}$  and 130 scatterers per  $\text{mm}^3$  are randomly distributed in the phantom. Five cardiac myofibers are set with a size of 2 mm in length and 0.045 mm in diameter. Three of the same reflection amplitude options are chosen for different image quality. All fibers are set at the known positions and arranged perpendicularly to the ultrasound beam directions in the images. During simulated ultrasound image acquisition, the imaging parameters for 21 MHz images are set as: center frequency is 21 MHz, sampling rate is 100 MHz, and focus depth is 16 mm. The imaging parameters for 40 MHz images are set as: center frequency is 40 MHz, sampling rate is 200 MHz, and focus depth is 7 mm. After the RF data acquisition, all data are log-compressed into gray scale images in the dynamic range of 60 dB.

Moreover, contrast-to-noise ratio (CNR) in the log-compressed image is utilized to indicate the noise level in the simulated images. The definition of CNR is (Thitaikumar *et al* 2007):

$$\text{CNR} = \frac{I_{mf} - I_{bg}}{(\text{Var}_{mf} + \text{Var}_{bg})^{1/2}}$$

where  $I_{mf}$  is the average gray scale intensity of myofibers in the image and  $\text{Var}_{mf}$  is its corresponding variance.  $I_{bg}$  is the average gray scale intensity of the background and  $\text{Var}_{bg}$  is its corresponding variance.

### 2.3. Myofiber extraction method

After data acquisition, a two-step multiscale image decomposition approach is proposed to extract the cardiac myofiber orientations from these images. Because we focus on the myofiber orientations, the tissue regions without myofibers were manually neglected. Figure 1 illustrates the whole flowchart of the fiber extraction method. The HFU images have serious speckle noise as shown in figure 4(b), which increases the difficulty of extracting myofiber structures. Hence, it is necessary to decrease this noise before fiber orientation extraction. On the other hand, although the fiber structures are bright in the images, the size of the small myofibers is similar to that of the noise. It is not trivial to distinguish fibers from noise. Therefore, the two-step multiscale image decomposition approach is proposed to solve this problem. The difference between both decompositions is the filters that boost different components of the signals.

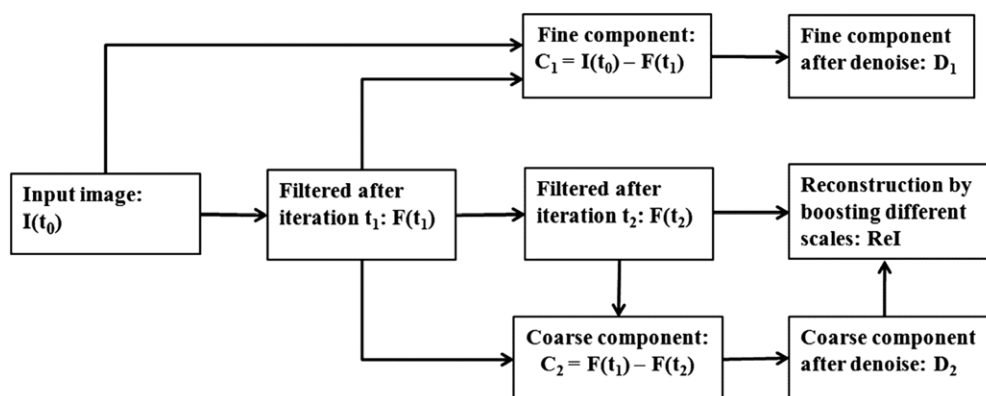


Figure 2. Flowchart of the two-step multiscale image decompositions.

The general procedure for each multiscale decomposition step is illustrated in figure 2. First, different scaled images  $F(t_1)$  and  $F(t_2)$  are calculated by nonlinear diffusion filters with different iteration times  $t_1$  and  $t_2 (t_1 < t_2)$ . Then, the input image is decomposed into different components  $D_1$  and  $D_2$  at different scales. After a threshold denoising for each component, the processed image is reconstructed by boosting the selected scales. The reconstructed image  $ReI$  is as follows:

$$ReI = k_1 \cdot D_1 + k_2 \cdot D_2 + (1 - k_1 - k_2) \cdot F(t_2), \tag{1}$$

where both  $k_1$  and  $k_2$  are the weighting parameters.

Figure 3(a) shows an original HFU image of LV tissue. The whole procedure of the fiber orientation extraction method is illustrated in figure 3. It contains three main steps: (1) multiscale decomposition with NLADF, (2) multiscale decomposition with CEDF, and (3) fiber extraction. The details are presented as follows.

**2.3.1. Multiscale decomposition with NLADF.** In the first multiscale decomposition step, an NLADF is utilized to decrease the speckle noise in the HFU images. The filtering method is based on the diffusion equation framework by considering anisotropic diffusion tensors. It has the advantage of decreasing noise but keeping the significant parts of the image content, typically edges, lines or other details, which are useful for the myofiber extraction. This filter is particularly suitable for the purpose of decreasing the speckle noise but keeping the main orientation information on ultrasound images. Its equation can be written as follows (Perona and Malik 1990):

$$I(\bar{x}, t)_t = div (c(\bar{x}, t) \cdot \nabla I(\bar{x}, t)), \quad t \geq 0, \tag{2}$$

where  $I$  is the intensity at the 2D space location  $\bar{x}$ ,  $t$  is the diffusion time and represents iteration steps,  $\nabla$  is the gradient operator in the space domain, and  $c$  is the diffusion tensor decided by both space and time domain.  $c$  is defined as:

$$c(\bar{x}, t) = \frac{1}{1 + \left(\frac{\|\nabla I(\bar{x}, t)\|}{K}\right)^2}, \tag{3}$$

where  $K$  is a constant value.

The original image as shown in figure 3(a) is smoothed twice by the NLADF as shown in figures 3(b), (c). Both the fine scale component  $D_1$  in figure 3(d) and the coarse scale

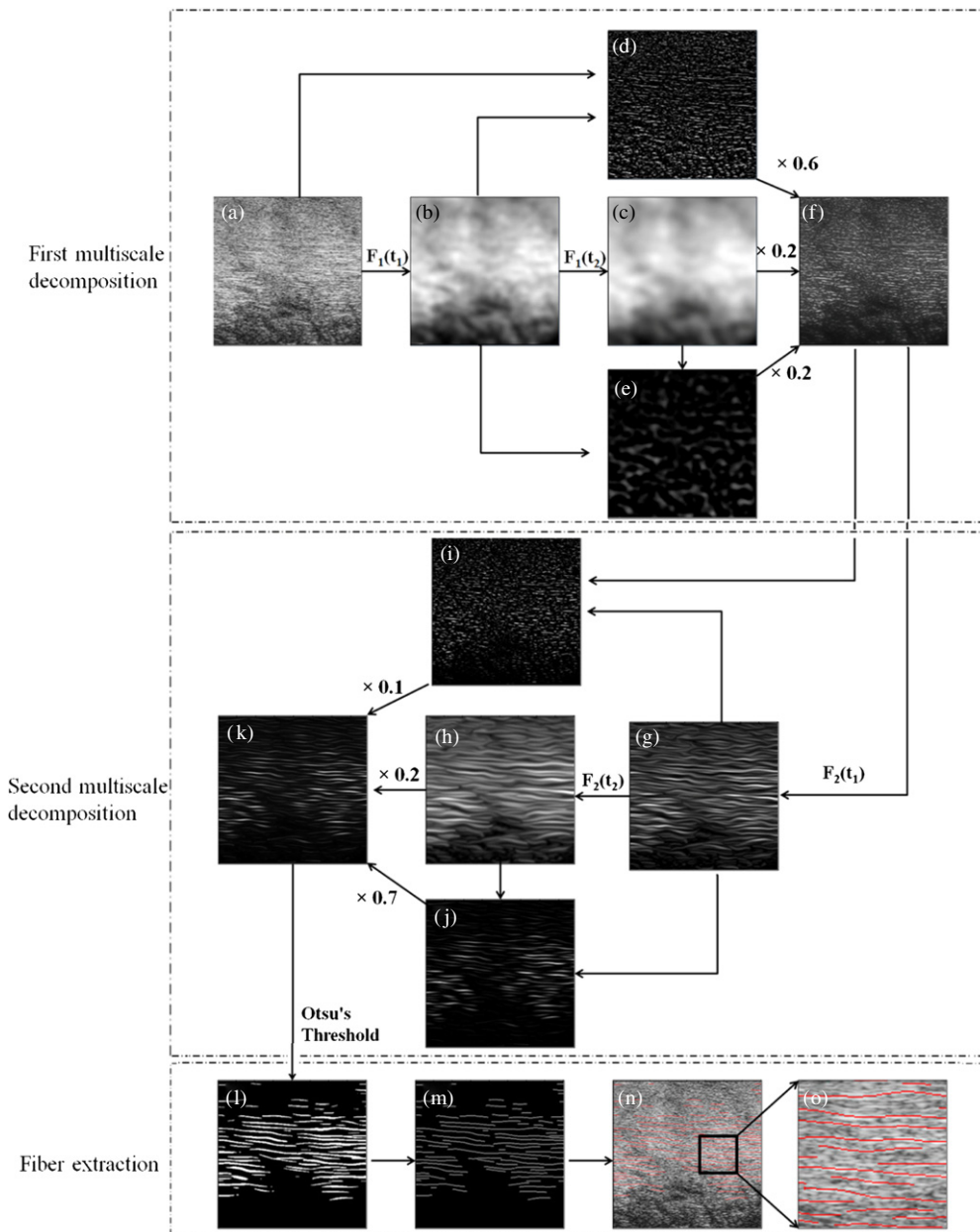


**Figure 3.** Extraction of cardiac fiber orientations of tissue from the left ventricular free wall. (a) The original HFU images. (b)–(f) Processed images of multiscale decomposition of the first filter ( $F_1$ )—NLADF. (g)–(k) Processed images of multiscale decomposition of the second filter ( $F_2$ )—CEDF. (l) Binary image after the Otsu's thresholding processing. (m) Skeleton extraction. (n)–(o) Final extracted myofiber orientations laid over the original image to show the estimated fiber orientations.

component  $D_2$  in figure 3(e) are generated separately. During this step, both components are denoised by setting the negative value as zero because the myofiber structure is generally brighter than other parts in the image. After this decomposition and denoising processes, a

reconstructed image  $ReI_1$  in figure 3(f) is obtained with a larger weighting parameter of 0.6 to boost the fine scale component on the image.

After the first multiscale decomposition with NLADF, the speckle noise in the image is decreased and the fiber structures, as shown in figure 3(f), are enhanced compared with the original images in figure 3(a). However, some of these enhanced fiber structures are still disconnected because of the speckle noise during imaging, which misleads the extraction of fiber orientation. In order to overcome these disconnections in the denoised image, the second multiscale decomposition with CEDF is applied in the following step.

**2.3.2. Multiscale decomposition with CEDF.** CEDF, steered by a structure tensor, has been used to complete interrupted lines and to enhance fiber structures in images (Weickert 1999). It is similar to the diffusion filter as described in equation (2) but with a different diffusion tensor. Considering equation (2), the diffusion tensor  $c$  is replaced by adapting the structure tensor  $J$ , whose definition is as follows (Weickert 1999):

$$J(\nabla I) = K_\rho * (\nabla I \cdot \nabla I^T), \quad (4)$$

with  $K_\rho$  a Gaussian weighting function with sigma  $\rho$ . If we calculate the eigenvalues  $\mu_1, \mu_2 (\mu_1 > \mu_2)$  and the corresponding eigenvectors  $\bar{V}_1, \bar{V}_2$  of the structure tensor, the localized image orientations can be represented as its eigenvectors. Based on them, the diffusion function can be rewritten with the following structure tensor:

$$I_t = \text{div}(D\nabla I), \quad (5)$$

where the diffusion tensor  $D$  is constructed with the same eigenvectors:

$$D = [\bar{V}_1 \quad \bar{V}_2] \cdot \begin{bmatrix} \lambda_1 & 0 \\ 0 & \lambda_2 \end{bmatrix} \cdot [\bar{V}_1 \quad \bar{V}_2]^T, \quad (6)$$

and its eigenvalues are given as:

$$\lambda_1 = \alpha, \quad \lambda_2 = \begin{cases} \alpha + (1 - \alpha) \exp\left(\frac{-C}{(\mu_1 - \mu_2)^2}\right), & \mu_1 \neq \mu_2 \\ \alpha, & \mu_1 = \mu_2 \end{cases}, \quad (7)$$

here  $C > 0$  is a threshold and  $\alpha \in (0, 1)$  is a small regularization parameter that keeps the diffusion tensor uniformly positive definite.

The reconstructed image in figure 3(f) is filtered twice by the CEDF as shown in figures 3(g), (h). Both the fine scale component  $D_1$  in figure 3(i) and the coarse scale component  $D_2$  in figure 3(j) are generated separately. Similar to the first decomposition step, both components are denoised and the enhanced image  $ReI_2$  in figure 3(k) is reconstructed.

Using structure tensor and multiscale decomposition, CEDF has the specific ability to enhance fiber structures and their orientations. The comparison between the original and processed images shows the effect of the processing, seen in figures 3(f) and (k).

**2.3.3. Fiber extraction.** After the two-step multiscale decomposition in figures 3(a)–(k), the final processed results are first transformed into binary images (figure 3(l)) based on its Otsu' threshold (Otsu 1979). Then, their orientations are finally extracted from this binary image using a skeleton extraction method (Au *et al* 2008), as shown in figure 3(m). Figure 3(m) and its enlarged section figure 3(o) demonstrate the final extracted cardiac myofiber orientations (red lines) overlaid on the original input image.

## 2.4. Evaluations

Quantitative performance assessment of the method is conducted by comparing the results with the corresponding gold standard for evaluation of classification and segmentation (Wang and Fei 2012, Mafi *et al* 2012, Qin *et al* 2009, Lv *et al* 2011). In this study, the known setting in a simulated image or manual identification of myofibers in a real image was used as the gold standard to evaluate the automatic extraction method. Mean absolute distance (MAD) and the Hausdorff distance (HD) are applied to quantitatively assess the performance of the proposed method. Suppose  $A$  and  $B$  are fiber orientations of automatic and manual results, respectively. They are represented by point sets:  $A = \{a_1, a_2, \dots, a_m\}$  and  $B = \{b_1, b_2, \dots, b_n\}$ , and their MAD and HD are defined as follows:

$$\text{MAD}(A, B) = \frac{1}{2} \left\{ \frac{1}{m} \sum_{i=1}^m d(a_i, B) + \frac{1}{n} \sum_{j=1}^n d(b_j, A) \right\}, \quad (8)$$

$$\text{HD}(A, B) = \max \left\{ \max_i \{d(a_i, B)\}, \max_j \{d(b_j, A)\} \right\}, \quad (9)$$

where  $d(a_i, B) = \min_j \|b_j - a_i\|$ . MAD can supply the global matching measurements and HD can supply the local similarity between automatic and manual results.

## 3. Results

### 3.1. Histological validation of cardiac myofiber orientations

Tissue from the left ventricular free wall of a porcine heart was used to verify the feasibility of imaging cardiac myofibers by HFU. Its shape was designed as a triangle as shown in figure 4(a). The bright boundaries of the triangle can be identified in the ultrasound images in figure 4(b) and also from the stained histology slide in figure 4(c). From the enlargement of the histology slide in figure 4(d), the myofibers in the tissue are clearly visible on the image. Thus, the corresponding bright lines in figure 4(b) indicate the myofiber orientations. Furthermore, although there were deformations during the histologic processing, figure 4(d) shows that the horizontal myofiber orientations mainly correspond to those fiber-structure orientations as shown in the enlarged region of the ultrasound image in figure 4(b). This experiment demonstrated that although it was relatively difficult to identify each single myofiber in the cardiac tissue, the local myofiber orientations could be still identified as groups of bright fiber-structures using HFU imaging.

### 3.2. Estimations of the simulated phantoms

Six different simulated HFU images are shown in figure 5, which simulate both skeletal and cardiac fiber images with different CNRs: 1.34, 1.04 and 0.77 for skeletal images; 2.20, 1.28 and 1.04 for cardiac images. To validate the performance of our proposed method (M3), we compared its results with those extracted by two other methods: a direct method by thresholding and skeleton extraction (M1), and a method of first smoothing the image by SRNDF and then extracting the fiber by thresholding and skeleton extraction (M2). The estimated fibers in the six images, which were extracted by these three methods, are illustrated in figure 5 as red lines in the images. Figures 5(b1)–(b6) show the results of M1, figures 5(c1)–(c6) show the results of M2 and figures 5(d1)–(d6) show the results of M3. It can be seen that the results of our proposed method M3 perform better than those from the other two methods. Especially for both images with lower CNRs (figures 5(a3), (a6)), the performance of our proposed method is

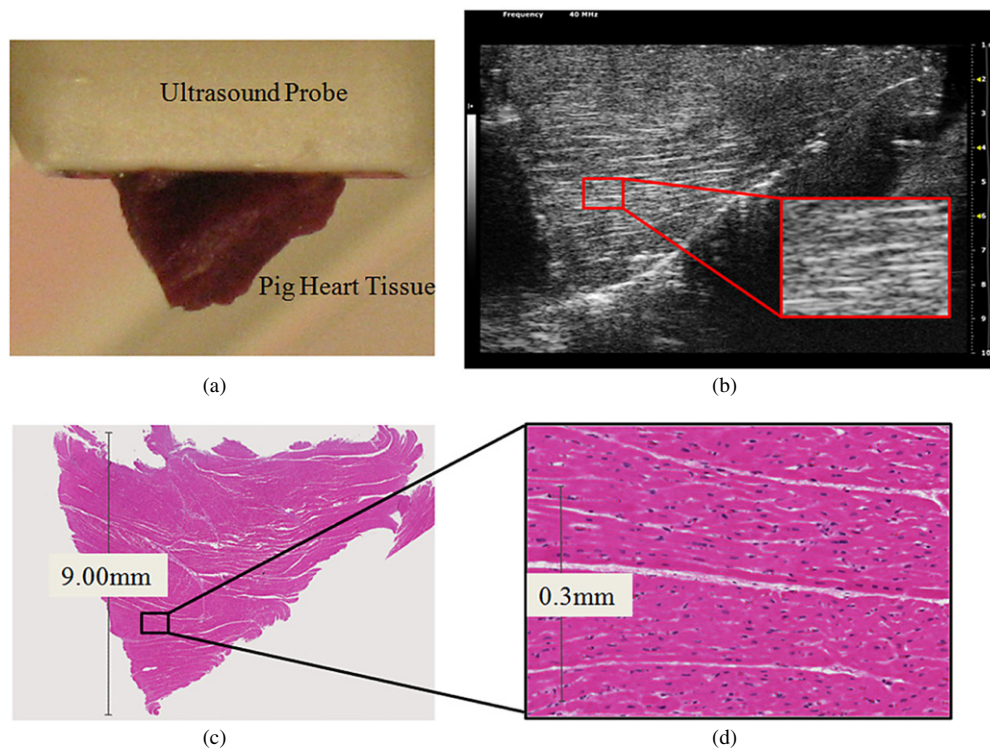


**Figure 4.** Comparison between HFU image and the stained histology slide. (a) The specifically shaped tissue from the left ventricle wall of a porcine heart during ultrasound imaging. (b) The corresponding ultrasound image. (c) The corresponding histological slide. (d) The enlargement of one small region from the histological slide.

**Table 1.** Evaluation of the extraction results from the simulated fiber images compared with the ground truth.

Phantoms	Mean absolute distance ( $\mu\text{m}$ )			Hausdorff distance ( $\mu\text{m}$ )		
	**M1	**M2	**M3	M1	M2	M3
*Image 1	50	50	10	850	830	140
*Image 2	90	90	27	2070	1400	276
*Image 3	184	240	44	1544	1175	807
*Image 4	20	20	8	530	150	80
*Image 5	80	60	20	630	1030	440
*Image 6	109	243	42	715	2196	499
Mean $\pm$ Std	89 $\pm$ 56	117 $\pm$ 99	25 $\pm$ 15	1057 $\pm$ 613	1130 $\pm$ 674	374 $\pm$ 268

\*Image 1, 2 and 3 are the simulated 21 MHz skeletal fiber images with different CNRs 1.59, 1.35 and 0.77, respectively. Image 4, 5 and 6 are the simulated 40 MHz cardiac fiber images with different CNRs 2.20, 1.28 and 1.04, respectively.

\*\*M1 is the method that uses thresholding and skeleton extraction. M2 is the method that first smooths the images by speckle reducing anisotropic diffusion filter and then extracts the fiber orientation by thresholding and skeleton extraction. M3 is our proposed method.

much better than the other two methods. This conclusion is also supported by the quantitative analysis results in table 1. Both evaluation parameters of MAD and HD demonstrate that the errors occurring in each simulated image by our method (M3) are lower than half of the other two methods.

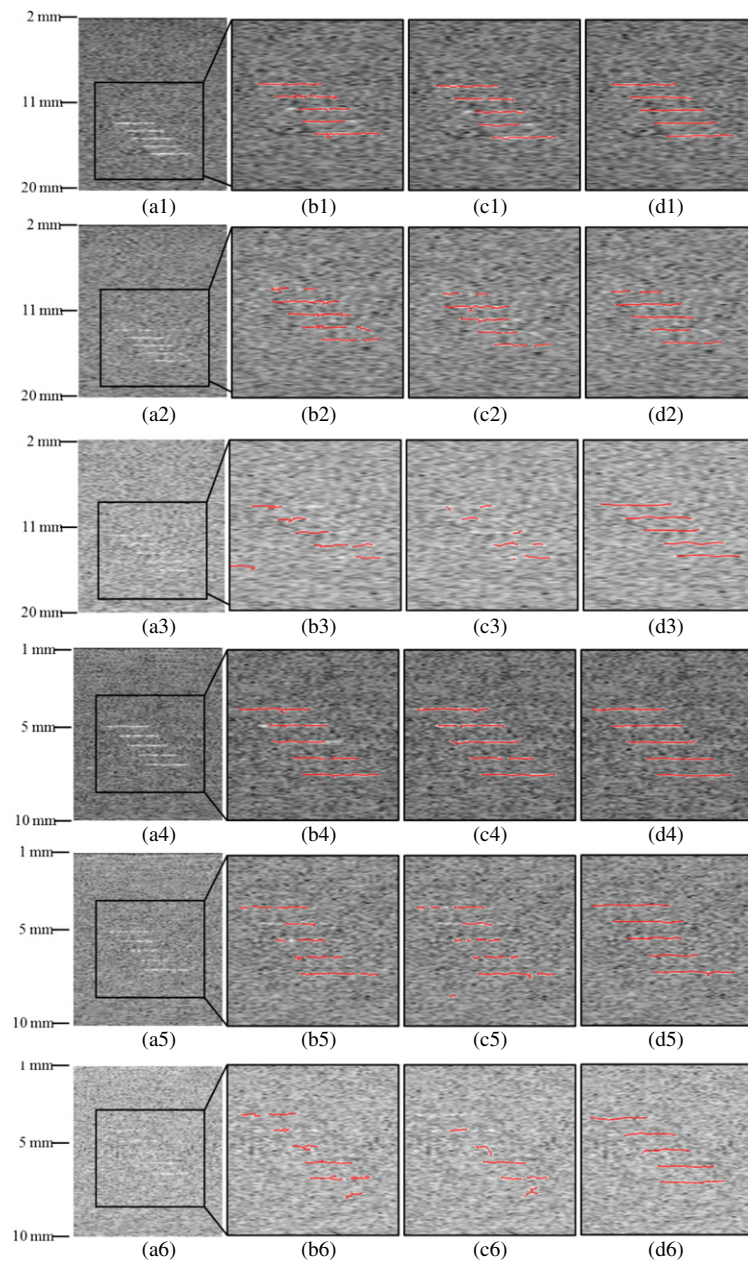


**Figure 5.** Fiber extraction from four simulated ultrasound images. (a1) was imaged by the 21 MHz scanner with the CNR of 1.34. (a2) was imaged by the 21 MHz scanner with the CNR of 1.04. (a3) was imaged by the 21 MHz scanner with the CNR of 0.77. (a4) was imaged by the 40 MHz scanner with the CNR of 2.20. (a5) was imaged by the 40 MHz scanner with the CNR of 1.28. (a6) was imaged by the 40 MHz scanner with the CNR of 1.04. (b1)–(b6) show the results of the direct method by thresholding and skeleton extraction, Figures (c1)–(c6) show the results of the method that first smooths the image by speckle reducing anisotropic diffusion filter. (d1)–(d6) show the results of our proposed method. The red lines indicate the extracted fibers.

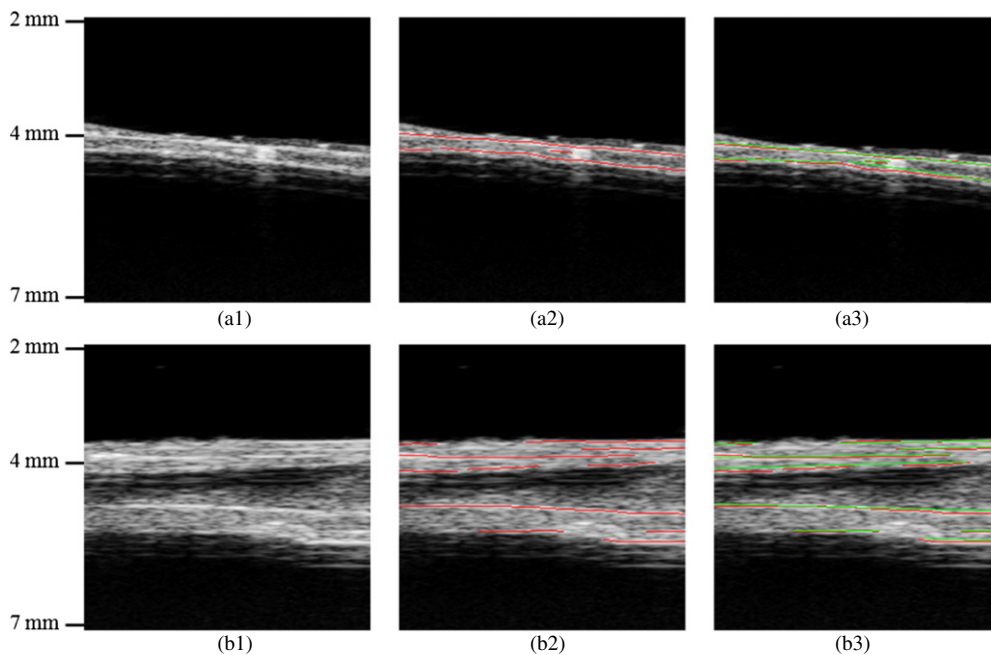


**Figure 6.** Comparison of myofiber orientations groups between the automatic and manual results in three myofiber tissue phantoms. (a1) and (b1) are the original ultrasound images. (a2) and (b2) are their corresponding extraction results (red lines) extracted by the proposed method. (a3) and (b3) show the myofiber orientations from the proposed method (red lines) and those from the manual results (green lines).

**Table 2.** Evaluation of the extraction results of the excised cardiac fiber phantoms compared with the manual gold standard.

Phantoms	Mean absolute distance ( $\mu\text{m}$ )			Hausdorff distance ( $\mu\text{m}$ )		
	*M1	*M2	*M3	M1	M2	M3
Single fiber	150	210	20	1060	1740	90
Two fibers	280	280	20	1740	2840	150
Mean	220	250	20	1400	2290	120

\*M1, M2 and M3 are the same as those in table 1.

### 3.3. Estimations of the excised fiber phantoms

Two HFU images of excised cardiac fiber bunches are shown in figures 6(a1), (b1). Each bunch contained several myofibers, and those appeared as brighter line structures in both images. These fibers were extracted by our proposed method as the red lines shown in figures 6(a2), (b2). Moreover, in order to quantitatively evaluate the extraction errors, the automatic extraction results were compared with the manual drawings performed by an expert. Figures 6(a3), (b3) demonstrate that the extracted results by the proposed method M3 are closer to the manual ones, which are shown as green lines in the figures. Similar to the simulated image experiment, we also utilized the other two methods M1 and M2 to process these excised fiber images in order to validate the performance of the proposed method. Table 2 shows the quantitative results of all three extractions on both phantoms. The mean MAD and HD of our proposed

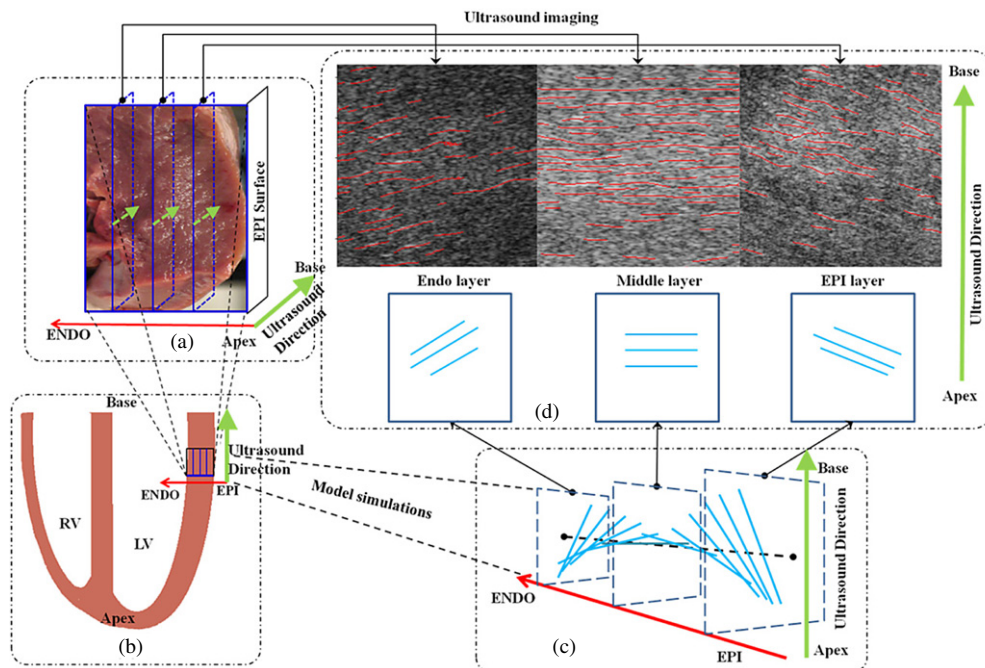


**Figure 7.** A comparison of different layer orientations between HFU results and model simulations (Savadjiev *et al* 2012). (a) Picture of the excised specimen from left ventricular free wall, which was imaged by ultrasound three times. (b) Diagram of the heart ventricles: left ventricle (LV) and right ventricle (RV) and the specimen in (a) was excised from LV free wall. (c) Myofiber orientations of the excised specimen from epicardium (EPI) to endocardium (ENDO) based on model simulations. (d) Similarities between the different layer orientations of the excised specimen extracted from ultrasound images by our proposed method and the ones from model simulations. The red arrow lines indicate the direction from EPI to ENDO of the free wall, the green arrow lines indicate the ultrasound imaging direction from apex to base of the heart, and three blue rectangles indicate the three different ultrasound imaging planes.

method are 20 and 120  $\mu\text{m}$ , respectively. On the contrary, the evaluation results of the other two methods are much higher, more than 200  $\mu\text{m}$  for the mean MAD and more than 1000  $\mu\text{m}$  for the mean HD.

#### 3.4. Extracted myofiber orientations in muscular tissue images

First, the myofiber orientations of heart tissues were extracted from 2D ultrasound images. Three different layers (outer, middle, and inner) of tissue from the LV free wall were imaged by the HFU imaging. The experimental scenario was illustrated in figure 7(a). The ultrasound probe was placed on the surface near the apex of the heart, which was imaged three times from epicardium to endocardium. The orientations of different layers were extracted from these ultrasound images, as shown in figure 7(d). From the images, the orientations of the three layers are different: the middle layer is parallel, and the other layers are perpendicular to each other. Furthermore, the intensity in the middle layer is brighter than the others because of the anisotropic character of the ultrasound images. Although the geometric structures and orientations of cardiac myofibers are complicated, simulation from DTI data and a generalized

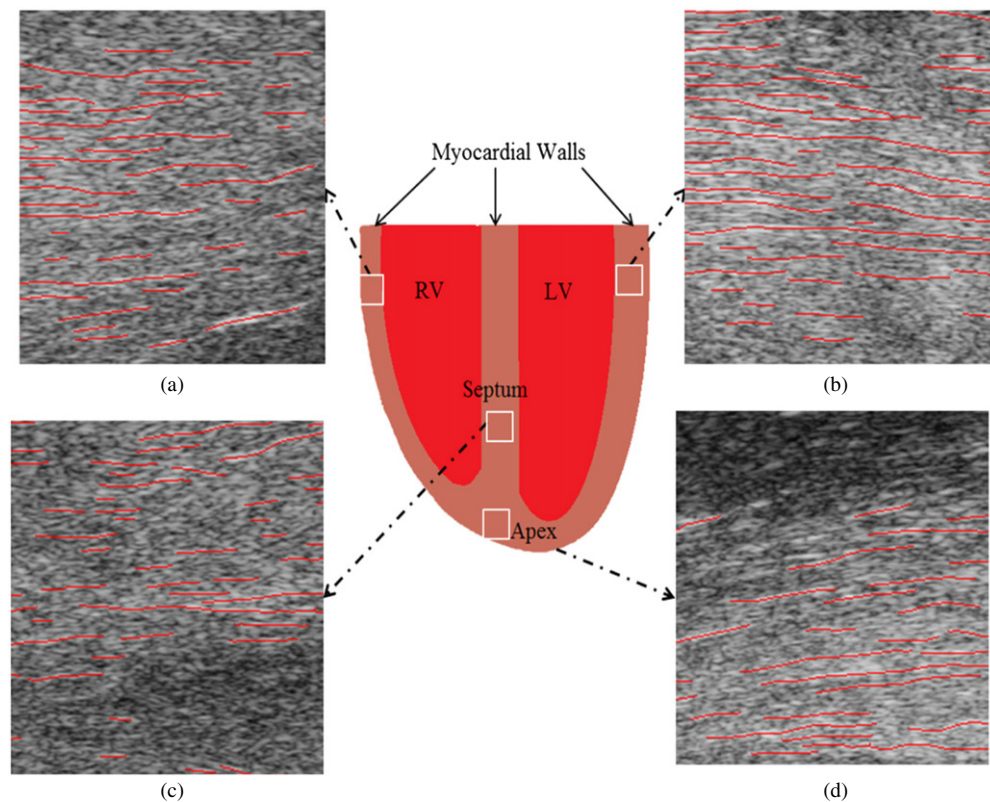


**Figure 8.** Cardiac myofiber orientations extracted by the proposed method from the HFU images of four different specimens of different ventricle regions. (a) Free wall of right ventricle. (b) Free wall of left ventricle. (c) Ventricle septum wall. (d) Apex.

helicoid model were used to study the myofiber layers (Lombaert *et al* 2012, Savadjiev *et al* 2012, Vadakkumpadan *et al* 2012). It has been reported that the general orientations can be divided into different layers, with the myofiber orientations continuously changing along the depth (Savadjiev *et al* 2012). The model simulation was illustrated in figure 7(c). In order to validate the results derived from ultrasound images, the orientations of the three layers in figure 7(a) were compared with the ones simulated by the model. Figure 7(d) demonstrates that the orientations of the three different layers were similar to those of the model simulations.

Figure 8 shows the myofiber orientations of four different myocardial tissue specimens from different parts of the heart ventricles. There are differences between the orientation patterns of the four tissue specimens, especially the helical orientation at the apex. These results indicated the possibility of using HFU to image different cardiac fibers of the heart ventricles and also of using our method to quantitatively analyze their cardiac fiber orientations.

Second, myofiber fiber orientations of skeletal muscles were also extracted. Both images of the arm and leg skeletal muscles were acquired with the 21 MHz probe. The fiber orientations were extracted by the proposed two-scale image decomposition procedures. Figure 9 demonstrates the feasibility of the proposed method to extract skeletal myofiber orientations from 2D ultrasound images, where figure 9(a1) is the muscle image of the

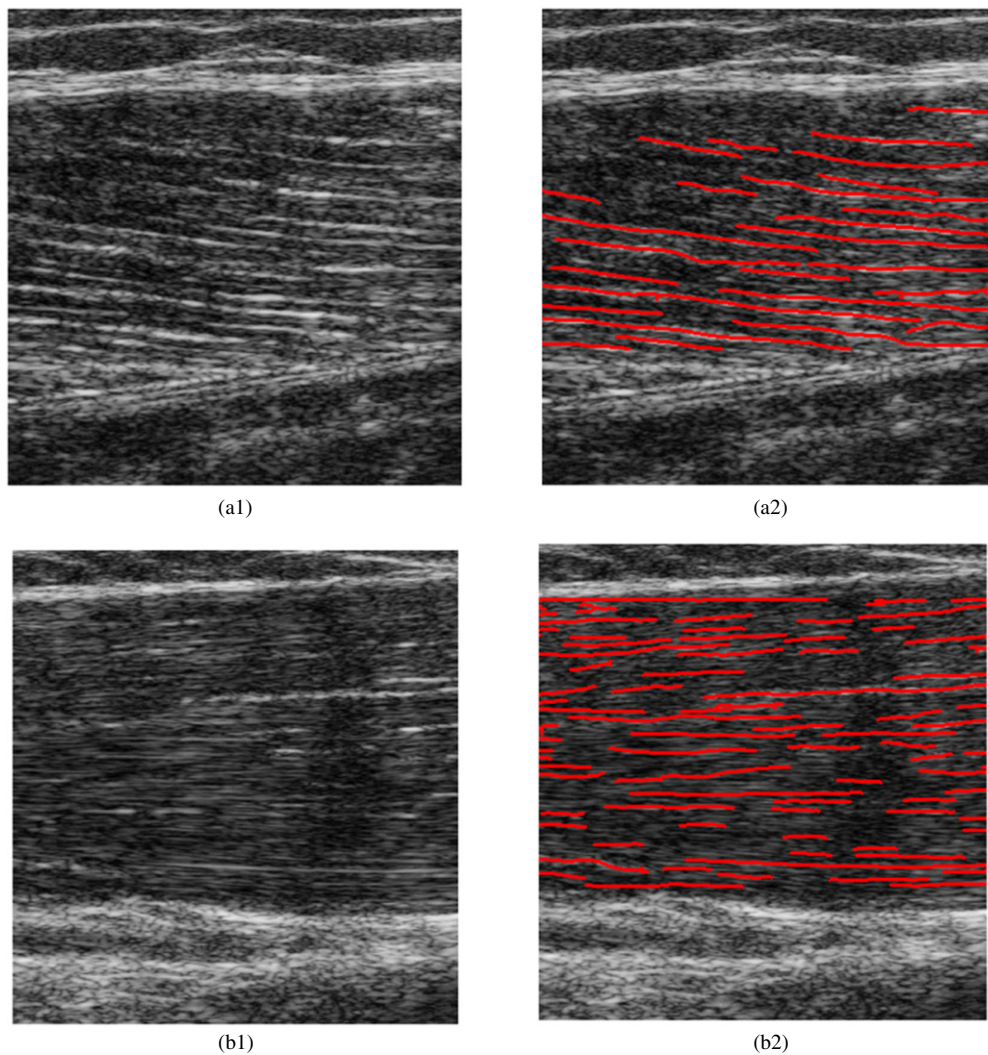


**Figure 9.** Myofiber orientations extracted from the 2D ultrasound of skeleton muscles. (a1) The ultrasound image of gastrocnemius muscles in the right human leg. (a2) The extracted myofiber orientations of (a1). (b1) The ultrasound image of the brachioradialis muscles in the left forearm. (b2) The extracted myofiber orientations of (b1).

gastrocnemius in the right human leg and figure 9(b1) is the image of the brachioradialis in the left forearm.

#### 4. Discussion and conclusions

This paper proposed an automatic method to extract myofiber orientations from HFU images, which included two-step multiscale image decompositions. The results from simulated images, excised fiber phantoms, specimens of porcine hearts and human skeletal muscle images

demonstrated that the proposed method could extract both cardiac and skeletal myofiber orientations from the HFU images.

HFU scanners were selected in our experiments because of their ability to image small-scale myofiber structures. For example, it has been reported that the dimensions of single cardiac myocytes were 130–140  $\mu\text{m}$  in length and 18  $\mu\text{m}$  in diameter (Gerdes and Capasso 1995) and that their grouping fiber sheets were about 40  $\mu\text{m}$  in thickness, which are below the spatial resolution of the general clinical ultrasound imaging systems at low frequencies (<10 MHz). Thus, we chose the 40 MHz scanner to image the cardiac fibers due to its axis resolution of 40  $\mu\text{m}$ . Considering both the imaging depth and larger diameter of skeletal fibers (100  $\mu\text{m}$ ), we chose a 21 MHz scanner to image the skeletal fibers.

However, the HFU also brought additional problems in the fiber orientation extractions. The most severe one was that HFU led to vast number of scatter points in ultrasound images (Crosby *et al* 2009), as shown in figure 4(b). This decreased the image quality, resulting in low CNRs, and also led to difficulties in fiber orientation extractions. Moreover, because of the small diameters of myofibers, their continuous structures could also be interrupted and misled by the speckles of other scatter points, which made it more difficult to extract fiber orientations. Therefore, aiming at these problems, our two-scale decomposition method was proposed. Figure 5 demonstrates these problems and also shows the extracted results of our method and the other two methods for the images with different frequencies and different CNRs. The evaluations in tables 1 and 2 also quantitatively indicate that our proposed method performs better than other two methods. Furthermore, it can be seen from figure 5 and table 1 that the performances of the three methods become worse when the CNRs of the images decrease. But even so, the results of our proposed method are still the best in every image. That is because the first decomposition step of NLADF improves the fiber intensities among these speckle noises and because the second decomposition step of CEDF enhances the fiber orientations based on the first step, as demonstrated in figure 3 above.

During ultrasound imaging of myofibers, one should consider not only the fiber size but also the relationship between the fiber orientations and the ultrasound beam direction. This has been well investigated in cardiac ultrasound imaging at low frequencies (McLean and Prothero 1991, Holland *et al* 2005, Crosby *et al* 2009). It has been found that the fiber orientations affected the ultrasound image intensity: the fibers that are perpendicular to the ultrasound beam direction in the imaging plane were brightest and those that are parallel to the beam almost vanished. This relationship also works for the HFU imaging of myofibers. Thus, in our experiments, almost all fibers were perpendicular to the ultrasound beam direction for the purpose of imaging them clearly.

Our proposed myofiber orientation extraction method has several possible applications in both clinical and pre-clinical ultrasound imaging. First, the HFU imaging can be directly applied to skeletal muscle imaging *in vivo*, such as for diagnosis of muscular abnormalities in the legs and arms. Thus, it could be directly applied and may be able to provide quantitative analysis for clinical diagnosis, especially in pediatric clinics. In addition to providing the orientation of the skeletal muscles, our method can also provide their lengths, density and textures, which might be useful for clinical diagnosis. Second, our proposed method has demonstrated the feasibility of extracting cardiac fiber orientations from HFU *ex vivo*. Thus, it also has the potential to quickly image fiber orientations in cultured cardiac tissue patches (Radisic *et al* 2004) and in surgical ventricular restorations (Cirillo 2009) in the future. Finally, HFU imaging has been widely used in pre-clinical imaging of small animal hearts (Foster *et al* 2011). Thus, our proposed method for HFU imaging can provide automatic quantifications in pre-clinical imaging applications.

## Acknowledgments

The authors would like to thank Dr M Wagner and Dr R Jiang in the Department of Pediatrics and Dr Z Cong in the Department of Radiology and Imaging Sciences of Emory University for their valuable suggestions. This research is supported in part by NIH grants R01CA156775 and R21CA176684, Georgia Cancer Coalition Distinguished Clinicians and Scientists Award, and the Emory Molecular and Translational Imaging Center (NIH P50CA128301).

## References

- Akbari H and Fei B W 2012 3D ultrasound image segmentation using wavelet support vector machines *Med. Phys.* **39** 2972–84
- Au O K C, Tai C L, Chu H K, Cohen-Or D and Lee T Y 2008 Skeleton extraction by mesh contraction *ACM Trans. Graph.* **27** 44:1–10
- Bedi D G, Gombos D S, Ng C S and Singh S 2006 Sonography of the eye *Am. J. Roentgenol.* **187** 1061–72
- Bellah R 2001 Ultrasound in pediatric musculoskeletal disease—techniques and applications *Radiol. Clin. N. Am.* **39** 597
- Burgeth B, Didas S and Weickert J 2009 A general structure tensor concept and coherence-enhancing diffusion filtering for matrix fields *Math. Vis.* **4** 305–23
- Cetingul H E, Vidal R, Plank G and Trayanova N 2008 Nonlinear filtering for extracting orientation and tracing tubular structures in 2D medical images *IEEE Int. Symp. Biomed. Imaging* pp 260–3
- Choudhury A and Medioni G 2011 Perceptually motivated automatic sharpness enhancement using hierarchy of non-local means *ICCV Workshops* pp 730–7
- Cirillo M 2009 A new surgical ventricular restoration technique to reset residual myocardium's fiber orientation: the 'KISS' procedure *Ann. Surg. Innov. Res.* **3** 6
- Crosby J, Hergum T, Remme E W and Torp H 2009 The effect of including myocardial anisotropy in simulated ultrasound images of the heart *IEEE Trans. Ultrason. Ferroelectr. Freq. Control* **56** 326–33
- Dutt V and Greenleaf J F 1996 Adaptive speckle reduction filter for log-compressed B-scan images *IEEE Trans. Med. Imaging* **15** 802–13
- Fei B, Schuster D, Master V and Nieh P 2012 Incorporating PET/CT images into 3D ultrasound-guided biopsy of the prostate *Med. Phys.* **39** 3888
- Filoux E, Mamou J, Aristizabal O and Ketterling J A 2011 Characterization of the spatial resolution of different high-frequency imaging systems using a novel anechoic-sphere phantom *IEEE Trans. Ultrason. Ferroelectr. Freq. Control* **58** 994–1005
- Fleming C P, Ripplinger C B M, Webb B, Efimov I R and Rollins A M 2008 Quantification of cardiac fiber orientation using optical coherence tomography *J. Biomed. Opt.* **13** 030505
- Foster F S, Hossack J and Adamson S L 2011 Micro-ultrasound for preclinical imaging *Interface Focus* **1** 576–601
- Foster F S, Mehi J, Lukacs M, Hirson D, White C, Chaggares C and Needles A 2009 A new 15–50 MHz array-based micro-ultrasound scanner for preclinical imaging *Ultrasound Med. Biol.* **35** 1700–8
- Fukunaga T, Ichinose Y, Ito M, Kawakami Y and Fukashiro S 1997 Determination of fascicle length and pennation in a contracting human muscle *in vivo* *J. Appl. Physiol.* **82** 354–8 (PMID: 9029238)
- Galun M, Basri R and Brandt A 2007 Multiscale edge detection and fiber enhancement using differences of oriented means *IEEE ICCV* pp 1–8
- Gerdes A M and Capasso J M 1995 Structural remodeling and mechanical dysfunction of cardiac myocytes in heart failure *J. Mol. Cell. Cardiol.* **27** 849–56
- Gerig G, Kubler O, Kikinis R and Jolesz F A 1992 Nonlinear anisotropic filtering of MRI data *IEEE Trans. Med. Imaging* **11** 221–32
- Hodges P W, Pengel L H M, Herbert R D and Gandevia S C 2003 Measurement of muscle contraction with ultrasound imaging *Muscle Nerve* **27** 682–92
- Holland M R, Kovacs A, Posdamer S H, Wallace K D and Miller J G 2005 Anisotropy of apparent backscatter in the short-axis view of mouse hearts *Ultrasound Med. Biol.* **31** 1623–9
- Jensen J A and Svendsen N B 1992 Calculation of pressure fields from arbitrarily shaped, apodized, and excited ultrasound transducers *IEEE Trans. Ultrason. Ferroelectr. Freq. Control* **39** 262–7

- Kiesel K B, Uhl T L, Underwood F B, Rodd D W and Nitz A J 2007 Measurement of lumbar multifidus muscle contraction with rehabilitative ultrasound imaging *Manual Ther.* **12** 161–6
- Krogh T P, Fredberg U, Christensen R, Stengaard-Pedersen K and Ellingsen T 2013 Ultrasonographic assessment of tendon thickness, Doppler activity and bony spurs of the elbow in patients with lateral epicondylitis and healthy subjects: a reliability and agreement study *Ultraschall Med.* **34** 468–74
- Lombaert H, Peyrat J M, Croisille P, Rapacchi S, Fanton L, Cheriet F, Clarysse P, Magnin I, Delingette H and Ayache N 2012 Human atlas of the cardiac fiber architecture: study on a healthy population *IEEE Trans. Med. Imaging* **31** 1436–47
- Lv G, Yan G and Wang Z 2011 Bleeding detection in wireless capsule endoscopy images based on color invariants and spatial pyramids using support vector machines *IEEE EMBC* pp 6643–6
- Mademli L and Arampatzis A 2005 Behaviour of the human gastrocnemius muscle architecture during submaximal isometric fatigue *Eur. J. Appl. Physiol.* **94** 611–7
- Mafi J N *et al* 2012 Assessment of coronary artery calcium using dual-energy subtraction digital radiography *J. Digit. Imaging* **25** 129–36
- Martius P, Tech S, Stachs O and Guthoff R F 2010 Transpalpebral measurement of axial eye length. Use of contact B-scan sonography *Ophthalmologe* **107** 733–9
- McLean M and Prothero J 1991 Myofiber orientation in the weanling mouse heart *Am. J. Anat.* **192** 425–41
- Miyoshi T, Kihara T, Koyama H, Yamamoto S I and Komeda T 2009 Automatic detection method of muscle fiber movement as revealed by ultrasound images *Med. Eng. Phys.* **31** 558–64
- Moran C M, Pye S D, Ellis W, Janeczko A, Morris K D, McNeilly A S and Fraser H M 2011 A comparison of the imaging performance of high resolution ultrasound scanners for preclinical imaging *Ultrasound Med. Biol.* **37** 493–501
- Nilufar S, Ray N and Zhang H 2012 Object detection with DoG scale-space: a multiple kernel learning approach *IEEE Trans. Image Process.* **21** 3744–56
- Otsu N 1979 A threshold selection method from gray-level histograms *IEEE Trans. Syst. Man Cybern.* **9** 62–6
- Paquin D, Levy D and Xing L 2009 Multiscale registration of planning CT and daily cone beam CT images for adaptive radiation therapy *Med. Phys.* **36** 4–11
- Perona P and Malik J 1990 Scale-space and edge-detection using anisotropic diffusion *IEEE Trans. Pattern Anal.* **12** 629–39
- Pillen S and van Alfen N 2011 Skeletal muscle ultrasound *Neurol. Res.* **33** 1016–24
- Qin X, Cong Z and Fei B 2013a Automatic segmentation of right ventricular ultrasound images using sparse matrix transform and level set *Phys. Med. Biol.* **58** 7609–24
- Qin X, Cong Z, Jiang R, Shen M, Wagner M B, Kirshbom P and Fei B 2013b Extracting cardiac myofiber orientations from high frequency ultrasound images *Proc. SPIE* **8675** 867507
- Qin X, Wang S and Wan M 2009 Improving reliability and accuracy of vibration parameters of vocal folds based on high-speed video and electroglottography *IEEE Trans. Biomed. Eng.* **56** 1744–54
- Qin X, Wu L, Jiang H, Tang S, Wang S and Wan M 2011 Measuring body-cover vibration of vocal folds based on high frame rate ultrasonic imaging and high-speed video *IEEE Trans. Biomed. Eng.* **58** 2384–90
- Radisic M, Park H, Shing H, Consi T, Schoen F J, Langer R, Freed L E and Vunjak-Novakovic G 2004 Functional assembly of engineered myocardium by electrical stimulation of cardiac myocytes cultured on scaffolds *Proc. Natl Acad. Sci. USA* **101** 18129–34
- Savadjiev P, Strijkers G J, Bakermans A J, Piuze E, Zucker S W and Siddiqi K 2012 Heart wall myofibers are arranged in minimal surfaces to optimize organ function *Proc. Natl Acad. Sci. USA* **109** 9248–53
- Sengupta P P, Korinek J, Belohlavek M, Narula J, Vannan M A, Jahangir A and Khandheria B K 2006 Left ventricular structure and function: basic science for cardiac imaging *J. Am. Coll. Cardiol.* **48** 1988–2001
- Shi J, Zheng Y P, Huang Q H and Chen X 2008 Continuous monitoring of sonomyography, electromyography and torque generated by normal upper arm muscles during isometric contraction: sonomyography assessment for arm muscles *IEEE Trans. Biomed. Eng.* **55** 1191–8
- Subr K, Soler C and Durand F 2009 Edge-preserving multiscale image decomposition based on local extrema *ACM Trans. Graph.* **28** 147:1–9
- Tang S J and Tang X Y 2012 Statistical CT noise reduction with multiscale decomposition and penalized weighted least squares in the projection domain *Med. Phys.* **39** 5498–512
- Thitaikumar A, Krouskop T A and Ophir J 2007 Signal-to-noise ratio, contrast-to-noise ratio and their trade-offs with resolution in axial-shear strain elastography *Phys. Med. Biol.* **52** 13–28

- Vadakkumpadan F, Arevalo H, Ceritoglu C, Miller M and Trayanova N 2012 Image-based estimation of ventricular fiber orientations for personalized modeling of cardiac electrophysiology *IEEE Trans. Med. Imaging* **31** 1051–60
- Wang H and Fei B 2009 A modified fuzzy C-means classification method using a multiscale diffusion filtering scheme *Med. Imaging Anal.* **13** 193–202
- Wang H S and Fei B W 2012 An MR image-guided, voxel-based partial volume correction method for PET images *Med. Phys.* **39** 179–94
- Weickert J 1999 Coherence-enhancing diffusion filtering *Int. J. Comput. Vision* **31** 111–27
- Yongjin Z and Yong-Ping Z 2009 Enhancement of muscle fibers in ultrasound images using Gabor filters *IEEE Int., Ultrasonics Symp.* pp 2296–9
- Yu Y J and Acton S T 2002 Speckle reducing anisotropic diffusion *IEEE Trans. Image Process.* **11** 1260–70
- Zhou Y J and Zheng Y P 2008 Estimation of muscle fiber orientation in ultrasound images using revoting Hough transform (RVHT) *Ultrasound Med. Biol.* **34** 1474–81